CHINESE JOURNAL OF PHYSICS VOL. 50, NO. 5 October 2012

Time-Dependent Flow and Heat Transfer over a Stretching Cylinder

Sufian Munawar,[1,2,*] Ahmer Mehmood,[3] and Asif Ali[1]

[1]*Department of Mathematics, Quaid-i-Azam University, Islamabad 44000, Pakistan*
[2]*Department of Mathematics, School of Science & Technology, University of Management & Technology, Lahore, 54770, Pakistan*
[3]*Department of Mathematics (FBAS), International Islamic University, Islamabad, 44000, Pakistan*

(Received December 7, 2011; Revised January 19, 2012)

The unsteady laminar boundary-layer flow and heat transfer of a viscous fluid over a stretching cylinder is discussed in this work. To normalize the governing system of equations a proper set of similarity variables is used. Two types of thermal boundary conditions, prescribed surface temperature (PST) and prescribed heat flux (PHF), are taken into account for thermal analysis. The governing equations are solved using the homotopy analysis method, and the obtained series solution is found to be valid for the entire temporal and spatial domains and for certain ranges of the other physical parameters. The effects of various material parameters on different physical quantities, such as the coefficient of skin friction and the Nusselt number, are illustrated through graphs and tables.

PACS numbers: 44.20.+b, 44.05.+e, 47.15.Cb, 47.11.Bc

I. INTRODUCTION

A large number of practical implications of boundary-layer flow and heat transfer over solid surfaces have been found in many engineering and industrial processes. Therefore the theoretical understanding of flow and heat transfer phenomenon has attracted much curiosity among scientists and engineers over the last half century. In the manufacturing of various kinds of metallic and polymeric solids, such as metals and plastic, the raw material passes through a die in the molten state under high temperature for the extrusion process. At this phase, the material goes through linear stretching, elongating, and a cooling process. Such kinds of processes are very effective in the fabrication of metallic and plastic made equipment, such as cutting tools, electronic components in computers, rolling, the annealing of copper wires, etc. Furthermore, the cooling of a solid surface is an elementary tool for controlling the boundary-layer in many engineering and industrial applications. Due to these practical and realistic impacts, the problem of cooling of solid moving surfaces has become an area of attention for scientists and engineers. Pohlhausen [1] did the pioneering work to investigate the cooling problem for a flat plate, and formulated an expression for the coefficient of heat transfer. The analysis of the flow over a moving surface was initiated by Sakiadis [2]. Erickson *et al.* [3] and Tsou *et al.* [4] analyzed heat transfer in the flow

*Electronic address: sufian.munawar@hotmail.com

over a moving flat surface. Flow due to a stretching surface was discussed by Crane [5], and the exact solution for the problem was obtained. Furthermore, Crane *et al.* [6] scrutinized the heat transfer effects on the flow over a stretching surface. Afterwards, the work [5] was extended to three-dimensional flow by Wang [7]. Grubka and Bobba [8], Ali [9], and Elbashbeshy [10] investigated the heat transfer phenomenon over a uniformly stretching sheet. Takhar *et al.* [11] examined the effect of magnetohydrodynamic (MHD) fluid flow and heat transfer over a stretching surface and captured the results for two types of thermal boundary conditions, i.e., PST and PHF. Cortell [12] investigated the flow and heat transfer due to the nonlinear stretching of a flat surface. Ali and Mehmood [13] obtained the analytic solution for the flow over a stretching plate in a porous medium with suction and blowing effects.

The flow over a stretching cylinder was instigated by Wang [14], who studied the flow with heat transfer analysis over a stretching cylinder surrounded by a stationary fluid. Subsequently, many authors [15–19] examined numerous aspects of this idea and obtained similarity solutions. Brude [15] acquired the exact solution of equations for axisymmetric motion of the viscous fluid near a stretching cylinder. Ishak and Nazar [16] discussed the heat transfer effect on the flow over a stretching cylinder with the help of a numerical method. The effect of an electrically conducting fluid flow due to a stretching cylinder in the presence of suction/blowing was examined by Nazar *et al.* [17, 18], in which the numerical solution was obtained using the Keller-box method. Weidman and Ali [19] inspected the stagnation point flow over a stretching cylinder and discussed the effects of aligned and nonaligned radial stagnation flow. All of the above mentioned authors inspected various features of steady flow over a stretching cylinder. However, unsteadiness is an important phenomenon from both the theoretical and experimental viewpoints, and no actual flow state exists which does not involve some degree of unsteadiness. In this regard, authors [20–29] considered unsteady boundary-layer flow over impulsively moving surfaces. Takhar *et al.* [20] and Wang [21] considered the flow over a stretching sheet, and obtained results which are valid for small time. Pop [22] obtained a series solution for the unsteady boundary-layer flow over a stretching sheet by the perturbation method and illustrated a convergent result for large time. Recently Xu and Liao [23], Liao [24], Mehmood and Ali [25–28], and Ali and Mehmood [29] presented purely analytic solutions to the unsteady viscous boundary-layer flows which were valid in the whole temporal and spatial domains. Munawar *et al.* [30] discussed the analytic solution of unsteady non-similar flow over a moving cylinder in the free stream of a viscous fluid with the help of the homotopy analysis method (HAM). Recently, Munawar *et al.* [31] examined the unsteady flow over an oscillatory stretching cylinder with the help of a numerical finite difference scheme.

In the current study, our attention is focused on the unsteady flow and heat transfer of a viscous fluid over a stretching cylinder using two types of thermal boundary conditions, namely, PST (prescribed surface temperature) and PHF (prescribed heat flux). To obtain the solution of the considered problem we use the homotopy analysis method (HAM) proposed by Liao [32]. The fundamental idea of HAM was set out by Liao [33] in 1992 to get the analytic series solution for nonlinear differential equations. In 1997 Liao [34] established a novel form of the HAM equation by introducing a convergence control parameter. This

homotopy analysis method was successfully applied by numerous authors [23–29, 35–40] to solve highly nonlinear differential equations. To choose the best values of the convergence controlling parameter, Liao [41] proposed an optimized method based on squared residual errors. The useful feature of this method is that the convergence solution series is not dependent upon the small or large parameter and convergence rate, and the region can be controlled by the convergence control parameter.

II. MATHEMATICAL FORMULATION OF THE PROBLEM

Consider an unsteady two-dimensional boundary-layer flow of an incompressible viscous fluid due to an impulsively stretching cylinder of radius $R(t)$. The fluid far away from the cylinder is assumed to be at rest. Initially, for $\tau < 0$, both the fluid and the cylinder are at rest and held at constant temperature T_∞; then at $\tau \geq 0$ the cylinder stretches abruptly with velocity $u_w = u_0 x/L$ and the thickness of the cylinder decreases as a consequence, where u_0 and L are the velocity and the length of the stretching surface, respectively. The center of the surface is held fixed, and the surface of the cylinder is stretched along the axial direction x while the r-axis is normal to the surface of cylinder. Disregarding the viscous dissipation, the equations that govern the flow and heat transfer of the considered problem are

$$\frac{\partial u}{\partial x} + \frac{1}{r}\frac{\partial (rv)}{\partial r} = 0, \tag{1}$$

$$\frac{\partial u}{\partial \tau} + u\frac{\partial u}{\partial x} + v\frac{\partial u}{\partial r} = \frac{\nu}{r}\frac{\partial}{\partial r}\left(r\frac{\partial u}{\partial r}\right), \tag{2}$$

$$\rho Cp\left[\frac{\partial T}{\partial \tau} + u\frac{\partial T}{\partial x} + v\frac{\partial T}{\partial r}\right] = \frac{k}{r}\frac{\partial}{\partial r}\left(r\frac{\partial T}{\partial r}\right). \tag{3}$$

They are subject to the boundary conditions

$$u = u_w = \frac{u_0 x}{L}, \quad v = 0 \quad \text{at } r = R(t) \text{ for } \tau \geq 0, \tag{4}$$

$$u = 0 \text{ as } r \to \infty \text{ for } \tau \geq 0. \tag{5}$$

The corresponding initial conditions are

$$u = v = 0 \text{ and } T = T_\infty \text{ for } \tau < 0, \tag{6}$$

where u and v are the components of the velocity in the x and r-directions, respectively, and $R(t)$, the radius of cylinder, is a decreasing function of time. For the temperature field T two types of thermal boundary conditions, namely, PST and PHF are considered as

$$\text{PST case: } \left.\begin{array}{c} T(x,r,\tau) = T_\infty + T_0\left(\frac{x}{L}\right)^n \text{ at } r = R(t) \\ T(x,r,\tau) = T_\infty \text{ as } r \to \infty, \end{array}\right\} \text{ for } \tau \geq 0, \tag{7}$$

$$\text{PHF case:} \quad \left.\begin{array}{l} -k\frac{\partial T}{\partial r} = D\left(\frac{x}{L}\right)^n \text{ at } r = R(t) \\ T(x,r,\tau) = T_\infty \text{ as } r \to \infty, \end{array}\right\} \text{ for } \tau \geq 0, \tag{8}$$

where D is the wall heat flux coefficient and n the power of the heat flux distribution. If we take $n = 0$, Eqs. (7) and (8) represent the isothermal and isoflux boundary conditions, respectively. The velocity components in term of the stream function $\psi(x, r, \tau)$ can be written as

$$u = \frac{1}{r}\frac{\partial \psi}{\partial r}, \qquad v = -\frac{1}{r}\frac{\partial \psi}{\partial x}. \tag{9}$$

The above system of Eqs. (1)–(8) can be transformed into a dimensionless form by using the transformations [42]

$$\eta = \frac{(r^2 - R^2)}{2R}\sqrt{\frac{u_0}{\nu L \xi}}, \quad \psi = \sqrt{\frac{u_0 \nu \xi}{L}} Rx f(\eta, \xi), \quad t = \frac{u_0}{L}\tau, \quad \xi = 1 - e^{-t}, \tag{10}$$

and for the temperature field

$$\theta(\eta, \xi) = \frac{(T - T_\infty)}{T_0\left(\frac{x}{L}\right)^n} \text{ (for the PST case)}, \quad g(\eta, \xi) = \frac{(T - T_\infty)}{\frac{DR}{k}\left(\frac{x}{L}\right)^n} \text{ (for the PHF case)}. \tag{11}$$

Using the above transformations the governing equations (1)–(8) can be found as

$$(1 + 2\kappa\sqrt{\xi}\eta)f''' + 2\kappa\sqrt{\xi}f'' - \xi f'^2 + \xi f f'' + (1 - \xi)\left(\frac{\eta}{2}f'' - \xi\frac{\partial f'}{\partial \xi}\right) = 0, \tag{12}$$

$$(1 + 2\kappa\sqrt{\xi}\eta)\theta'' + 2\kappa\sqrt{\xi}\theta' + \Pr\left[\xi f\theta' - n\xi\theta f' + (1 - \xi)\left(\frac{\eta}{2}\theta' - \xi\frac{\partial \theta}{\partial \xi}\right)\right] = 0, \tag{13}$$

$$(1 + 2\kappa\sqrt{\xi}\eta)g'' + 2\kappa\sqrt{\xi}g' + \Pr\left[\xi f g' - n\xi g f' + (1 - \xi)\left(\frac{\eta}{2}g' - \xi\frac{\partial g}{\partial \xi}\right)\right] = 0, \tag{14}$$

along with the boundary conditions

$$f(0, \xi) = 0, \quad f'(0, \xi) = 1, \quad f'(\infty, \xi) = 0, \tag{15}$$

$$\theta(0, \xi) = 1, \quad \theta(\infty, \xi) = 0, \text{ (for the PST case)}, \tag{16}$$

$$g\prime(0, \xi) = -1, \quad g(\infty, \xi) = 0, \text{ (for the PHF case)}, \tag{17}$$

where $\Pr\,(= \mu Cp/k)$ is the Prandtl number and $\kappa\left(= \sqrt{\nu L/(R^2 u_0)}\right)$ is the curvature parameter; as κ approaches to zero the result for the flat plate case can be recovered. In deriving the above Eqs. (12)–(17) we have used the chain rules $\frac{\partial}{\partial \tau} = \frac{\partial \eta}{\partial \xi}\frac{\partial \xi}{\partial t}\frac{\partial t}{\partial \tau}\frac{\partial}{\partial \eta} + \frac{\partial \xi}{\partial t}\frac{\partial t}{\partial \tau}\frac{\partial}{\partial \xi}$

and $\frac{\partial}{\partial r} = \frac{\partial \eta}{\partial r}\frac{\partial}{\partial \eta}$ and prime denotes the partial differentiation with respect to η while keeping ξ constant.

The shear stress τ_w at the wall is given by

$$\tau_w = \mu \left.\frac{\partial u}{\partial r}\right|_{r=R} = \frac{4\mu u_0 x}{RL} f''(0,\xi), \tag{18}$$

and the coefficient of skin friction C_f reduces to

$$C_f = \frac{\tau_w}{\rho u_0^2} = \frac{2}{\xi Re_x} f''(0,\xi). \tag{19}$$

The heat transfer rate at the surface for the PST case is given by

$$q_w = -k \left.\frac{\partial T}{\partial r}\right|_{r=R} = -kA\left(\frac{x}{L}\right)^n \sqrt{\frac{u_0}{\nu L \xi}}\theta'(0,\xi). \tag{20}$$

The local Nusselt number Nu_x takes the form

$$Nu_x = \frac{q_w x}{k(T_0 - T_\infty)} = -\sqrt{\frac{Re_x}{\xi}}\theta'(0,\xi) \quad \text{(for the PST case)}, \tag{21}$$

and

$$Nu_x = \frac{q_w x}{k(T_0 - T_\infty)} = \sqrt{\frac{Re_x}{\xi}}\frac{1}{g(0,\xi)} \quad \text{(for the PHF case)}. \tag{22}$$

III. SOLUTION BY THE HAM

III-1. Detail of the method

The highly non-linear partial differential equations (12)–(17) are solved with the help of the homotopy analysis method (HAM). According to the nature of the boundary conditions the solution series can be assumed as

$$f(\eta,\xi) = \sum_{k=0}^{\infty}\sum_{m=0}^{\infty}\sum_{l=0}^{\infty} a_{m,l}^k \xi^k \eta^l e^{-m\eta}, \tag{23}$$

$$\theta(\eta,\xi) = \sum_{k=0}^{\infty}\sum_{m=0}^{\infty}\sum_{l=0}^{\infty} b_{m,l}^k \xi^k \eta^l e^{-m\eta}, \tag{24}$$

$$g(\eta,\xi) = \sum_{k=0}^{\infty}\sum_{m=0}^{\infty}\sum_{l=0}^{\infty} c_{m,l}^k \xi^k \eta^l e^{-m\eta}, \tag{25}$$

where $a^k_{m,l}$, $b^k_{m,l}$, and $c^k_{m,l}$ are the coefficients which arise in a series solution (23)–(25). Considering the boundary conditions, the initial guesses can be selected as

$$f_0(\eta,\xi) = 1 - e^{-\eta}, \qquad \theta_0(\eta,\xi) = g_0(\eta,\xi) = e^{-\eta}, \tag{26}$$

and we introduce linear operators of the form

$$\mathcal{L}_f = \frac{\partial^3}{\partial\eta^3} - \frac{\partial}{\partial\eta} \text{ and } \mathcal{L}_\theta = \mathcal{L}_g = \frac{\partial^2}{\partial\eta^2} - \frac{\partial}{\partial\eta}. \tag{27}$$

Using the governing Eqs. (12)–(14) we define the non-linear operators as:

$$\begin{aligned}\mathcal{N}_f[F(\eta,\xi;p))] &= (1+2\kappa\sqrt{\xi}\eta)F'''(\eta,\xi;p) + 2\kappa\sqrt{\xi}F''(\eta,\xi;p) + \xi F(\eta,\xi;p)F''(\eta,\xi;p)\\ &\quad -\xi\left(F'(\eta,\xi;p)\right)^2 + (1-\xi)\left(\frac{\eta}{2}F''(\eta,\xi;p) - \xi\frac{\partial F'(\eta,\xi;p)}{\partial\xi}\right),\end{aligned} \tag{28}$$

$$\begin{aligned}\mathcal{N}_\theta[\Theta(\eta,\xi;p))] &= (1+2\kappa\sqrt{\xi}\eta)\Theta''(\eta,\xi;p) + 2\kappa\sqrt{\xi}\Theta'(\eta,\xi;p)\\ &\quad -n\,\mathrm{Pr}\,\xi F'(\eta,\xi;p)\Theta(\eta,\xi;p) + \mathrm{Pr}\left[\xi F(\eta,\xi;p)\Theta'(\eta,\xi;p)\right.\\ &\quad \left.+(1-\xi)\left(\frac{\eta}{2}\Theta'(\eta,\xi;p) - \xi\frac{\partial\Theta(\eta,\xi;p)}{\partial\xi}\right)\right],\end{aligned} \tag{29}$$

$$\begin{aligned}\mathcal{N}_g[G(\eta,\xi;p))] &= (1+2\kappa\sqrt{\xi}\eta)G''(\eta,\xi;p) + 2\kappa\sqrt{\xi}G'(\eta,\xi;p)\\ &\quad -n\,\mathrm{Pr}\,\xi F'(\eta,\xi;p)G(\eta,\xi;p) + \mathrm{Pr}\left[\xi F(\eta,\xi;p)G'(\eta,\xi;p)\right.\\ &\quad \left.+(1-\xi)\left(\frac{\eta}{2}G'(\eta,\xi;p) - \xi\frac{\partial G(\eta,\xi;p)}{\partial\xi}\right)\right].\end{aligned} \tag{30}$$

According to the homotopy analysis method [32], the so called zeroth order deformation equation can be written as

$$(1-p)\mathcal{L}_f[F(\eta,\xi;p) - f_0(\eta,\xi)] = c_1 p\mathcal{N}_f[F(\eta,\xi;p))], \tag{31}$$

$$(1-p)\mathcal{L}_\theta[\Theta(\eta,\xi;p) - \theta_0(\eta,\xi)] = c_2 p\mathcal{N}_\theta[\Theta(\eta,\xi;p))], \tag{32}$$

$$(1-p)\mathcal{L}_g[G(\eta,\xi;p) - g_0(\eta,\xi)] = c_3 p\mathcal{N}_g[G(\eta,\xi;p))]. \tag{33}$$

Subject to the boundary conditions

$$F(\eta,\xi;p) = 0,\ F'(\eta,\xi;p) = 1,\ \Theta(\eta,\xi;p) = 1,\ G'(\eta,\xi;p) = -1 \text{ at } \eta = 0, \tag{34}$$

$$F'(\eta,\xi;p) = \Theta(\eta,\xi;p) = G(\eta,\xi;p) = 0 \text{ as } \eta\to\infty, \tag{35}$$

where $0 \neq c_i$, $i = 1,2,3$ are convergence control parameters and $p \in [0,1]$ is the embedding parameter related to the deformation mappings $F(\eta,\xi;p)$, $\Theta(\eta,\xi;p)$, and $G(\eta,\xi;p)$,

which deform continuously from $f_0(\eta,\xi)$, $\theta_0(\eta,\xi)$, and $g_0(\eta,\xi)$ to $f(\eta,\xi)$, $\theta(\eta,\xi)$, and $g(\eta,\xi)$, respectively, as p varies from 0 to 1.

For simplicity the remaining details of the method are suppressed here; the complete solution of the original differential equations (12)–(17) can be written in the form of an infinite series of functions, i.e.,

$$f(\eta,\xi) = f_0(\eta,\xi) + \sum_{m=1}^{\infty} f_m(\eta,\xi), \tag{36}$$

$$\theta(\eta,\xi) = \theta_0(\eta,\xi) + \sum_{m=1}^{\infty} \theta_m(\eta,\xi), \tag{37}$$

$$g(\eta,\xi) = g_0(\eta,\xi) + \sum_{m=1}^{\infty} g_m(\eta,\xi). \tag{38}$$

It is observed from the above analysis that each solution series (36)–(38) contains one unknown convergence control parameter c_i, with the help of which we can control and adjust the convergence rate and region of the series solution. To ensure a rapid convergence of the solution series, we use the optimal values of the convergence control parameters. To obtain the optimal values of c_i, we first calculate the relative errors e_f, e_θ, and e_g between two consecutive iterations, and then use the formula of average square relative error given by Liao [41]:

$$E_{1m} = \sqrt{\frac{1}{N+1}\sum_{j=0}^{N}(e_{fj})^2}, \quad E_{2m} = \sqrt{\frac{1}{N+1}\sum_{j=0}^{N}(e_{\theta j})^2}, \quad E_{3m} = \sqrt{\frac{1}{N+1}\sum_{j=0}^{N}(e_{gj})^2}, \tag{39}$$

where $e_{fj} = e_f(j\Delta\eta,\xi)$, $e_{\theta j} = e_\theta(j\Delta\eta,\xi)$, and $e_{gj} = e_g(j\Delta\eta,\xi)$ are the discretization of the continuous functions $e_f(\eta,\xi)$, $e_\theta(\eta,\xi)$, and $e_g(\eta,\xi)$ into N pieces by choosing $\Delta\eta = 0.2$ and $N = 50$ for the considered problem. The best values of c_i can be found by minimizing the square relative errors E_{im} using the first derivative law of Calculus.

III-2. Convergence and accuracy of the method

To analyze the convergence, accuracy, and efficiency of the series solution we have drawn various tables. To find the best values of the convergence control parameters c_i (for $i = 1,2,3$), the average square relative errors (39) are minimized using the direct command 'NMinimize' of the computational software Mathematica. At the 19th order of approximation the optimized value of $c_1 = -0.438$ is found with the relative error of 4.5763×10^{-5}, and at the 14th order of approximation the values of $c_2 = -0.507$ and $c_3 = -0.500$ are found with errors 2.61418×10^{-5} and 1.0291×10^{-4}, respectively. The square residual errors E_{im} (for $i = 1,2,3$) are calculated in Table I at the optimal values of

TABLE I: The square residual error E_{im} at different orders of approximation when $\kappa = 0.2$, $\xi = 0.1$, $\Pr = 1.0$, and $n = 1$ are kept fixed.

Order of approximation	E_{1m} at $c_1 = -0.4$	E_{2m} at $c_2 = -0.5$	E_{3m} at $c_3 = -0.5$
2	5.35360×10^{-2}	1.08961×10^{-2}	3.27548×10^{-2}
4	2.34695×10^{-2}	4.06847×10^{-3}	1.87732×10^{-2}
6	1.01866×10^{-2}	1.46828×10^{-3}	1.05113×10^{-2}
8	4.40393×10^{-3}	5.19893×10^{-4}	5.87533×10^{-3}
12	8.19883×10^{-4}	6.07934×10^{-5}	1.83878×10^{-3}
14	3.53978×10^{-4}	2.61418×10^{-5}	1.02910×10^{-3}
16	1.55426×10^{-4}	3.97646×10^{-5}	5.83392×10^{-4}
20	6.58717×10^{-5}	9.71121×10^{-4}	8.19738×10^{-4}

the convergence controlling parameters c_i, and it is noted that as the order of approximation increases the corresponding residual errors decrease significantly.

To accelerate the convergence of the solution series (36)–(38) the homotopy-Padé approximation is utilized, and the tabulated results for $f''(0,\xi)$, $\theta'(0,\xi)$, and $g''(0,\xi)$ at the optimal values of the convergence controlling parameters c_i are listed in Table II. It is noticed from Table II that by choosing the optimal value of c_1 in the padé approximation of $f''(0,\xi)$ no correction is found up to the 5 decimal places after the 8th order of approximation. Similarly, no correction is needed after the 11th order of the Padé approximation for $\theta'(0,\xi)$ and $g''(0,\xi)$ up to the 5 decimal places.

TABLE II: Convergence table for the $[m/m]$ homotopy Padé approximation of $f''(0,\xi)$, $\theta'(0,\xi)$ and $g''(0,\xi)$, when $\kappa = 0.2$, $\xi = 0.1$, $\Pr = 1.0$ and $n = 1$ are kept fixed.

$[m/m]$	$f''(0,\xi)$	$\theta'(0,\xi)$	$g''(0,\xi)$
[2/2]	−0.63537	−0.63066	0.18456
[4/4]	−0.64050	−0.63860	0.19926
[6/6]	−0.64083	−0.63952	0.23678
[8/8]	−0.64098	−0.64135	0.20292
[10/10]	−0.64095	−0.64086	0.20334
[11/11]	−0.64095	−0.64083	0.20342
[12/12]	−0.64095	−0.64086	0.20342
[13/13]	−0.64095	−0.64086	0.20342

IV. NUMERICAL SOLUTION

The problem was also solved with the help of a numerical finite difference scheme to validate the analytic series solution. To use the finite difference method (FDM), we first transform the semi-infinite domain $\eta \in [0, \infty)$ into a finite domain $\zeta \in [0, 1]$ by using following transformation:

$$\zeta = \frac{1}{1+\eta}. \tag{40}$$

Using the above transformation, Eqs. (12)–(17) transform to a system of partial differential equations with bounded domain. To discretize this system we use following approximations for the spatial derivatives:

$$\frac{\partial f}{\partial \zeta} \approx \frac{f_{j+1} - f_{j-1}}{2\Delta\zeta} + O\left((\Delta\zeta)^2\right), \tag{41}$$

$$\frac{\partial^2 f}{\partial \zeta^2} \approx \frac{f_{j+1} - 2f_j + f_{j-1}}{(\Delta\zeta)^2} + +O\left((\Delta\zeta)^2\right), \tag{42}$$

$$\frac{\partial^3 f}{\partial \zeta^3} \approx \frac{f_{j+2} - 3f_{j+1} + 3f_j - f_{j-1}}{(\Delta\zeta)^3} + O(\Delta\zeta), \tag{43}$$

and the forward difference approximation for the temporal derivative. The discretized system of linear algebraic equations is solved with the help of the Gaussian elimination method for each time level. The complete details of the method are given in [31] and for simplicity are not included here.

The results obtained through both of the solution techniques are compared for various values of the parameters in Tables III, IV, and V. From these tables it is observed that both of the solutions are in good agreement up to 3 decimal places, therefore the validity of our analytic solution is verified.

V. RESULTS AND DISCUSSION

In this section, the effects of various parameters on the velocity, temperature, and other imperative physical quantities are scrutinized through graphs and tables. Figures 1–3 are plotted in order to see the effects of the curvature parameter κ on the velocity and temperature profiles for both types of thermal boundary conditions. From Figure 1 it is noticed that in the region $0 \leq \eta \leq 0.6$ the velocity of the fluid decreases as κ increases, and afterwards an opposite trend in the velocity profile is noticed and consequently the boundary-layer thickness increases. This behavior of the fluid velocity is due to the fact that as κ increases the radius of the cylinder decreases. Therefore the velocity due to

TABLE III: A comparison of the HAM solution with the numerical solution of $f''(0,\xi)$ for different values of the curvature parameter κ and ξ at the 13th order of Padé approximation.

κ	HAM results	Numerical results	HAM results	Numerical results
	$\xi = 0.2$	$\xi = 0.2$	$\xi = 0.4$	$\xi = 0.4$
0.0	−0.65611	−0.65652	−0.74578	−0.74578
0.2	−0.69813	−0.69910	−0.80232	−0.80251
0.5	−0.75824	−0.75816	−0.88255	−0.88260
1.0	−0.85228	−0.85233	−1.00695	−1.00713
1.5	−0.94979	−0.94983	−1.12328	−1.12331
2.0	−1.02509	−1.02515	−1.42200	−1.42200

TABLE IV: The Nusselt number $\sqrt{\mathrm{Re}_x}Nu_x$ for the PST case for different values of κ, Pr, and ξ, when $n = 1$.

Pr	κ	HAM results	Numerical results	HAM results	Numerical results
		$\xi = 0.2$	$\xi = 0.2$	$\xi = 0.5$	$\xi = 0.5$
1.0	0.0	1.46730	1.46025	1.11597	1.11601
	0.2	1.56097	1.56103	1.19745	1.19778
	0.5	1.69535	1.69684	1.32749	1.32756
	1.0	1.90591	1.90598	1.51757	1.51985
0.024	0.2	0.31479	0.31490	0.24375	0.24586
0.7		1.30755	1.30738	0.99968	0.99979
1.0		1.56097	1.56103	1.19745	1.19778
1.5		1.91033	1.91045	1.48253	1.48259

the surface area of the cylinder also reduces, and, as a consequence, the velocity gradient at the surface increases due to which the shear stress per unit area also increases. From Figure 1, it is also observed that by increasing the curvature of the cylinder the boundary-layer thickness increases significantly, as compared to the flat plate case. This is because of the fact that, unlike a flat plate, the momentum transport due to the phenomenon of convection takes place in the radial direction all around the cylinder.

Figures 2 and 3 depict the effect of the parameter κ on the temperature profiles (PST and PHF), respectively. It is noticed from here that the temperature profiles decrease in the neighborhood of the surface as κ increases, and afterwards rise dramatically and the thermal boundary-layer thickness increases. This behavior of the temperature profiles is seen to be due to the fact that as the radius of cylinder shrinks down the surface area that is

TABLE V: The Nusselt number $\sqrt{\mathrm{Re}_x}Nu_x$ for the PHF case when $n = 1$.

Pr	κ	HAM results $\xi = 0.2$	Numerical results $\xi = 0.2$	HAM results $\xi = 0.5$	Numerical results $\xi = 0.5$
1.0	0.0	1.37281	1.37467	1.01053	1.01209
	0.2	1.44594	1.44785	1.08224	1.08245
	0.5	1.54495	1.54367	1.18538	1.18569
	1.0	1.70764	1.70864	1.35456	1.35498
0.024	0.2	0.50137	0.50763	0.33048	0.32890
0.7		1.21205	1.21274	0.90250	0.90269
1.0		1.44594	1.44785	1.08224	1.08245
1.5		1.76682	1.76649	1.33278	1.33243

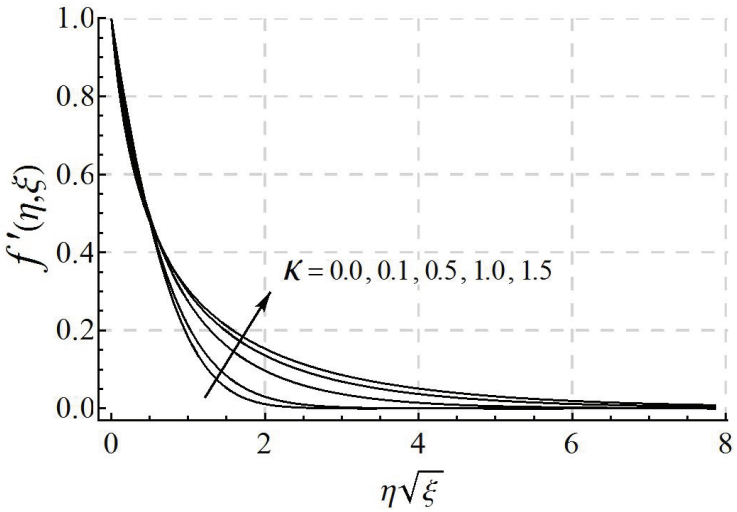

FIG. 1: Effects of the parameter κ on the velocity profile, when $\xi = 0.3$ is fixed.

in contact with the fluid also decreases. At this stage, it is important to mention here that heat is transferred to the fluid in modes: conduction at the surface, and convection in the region $\eta > 0$. Now, as the area of cylinder surface reduces, a slight fall in the temperature profile occurs near the surface of the cylinder, because less heat energy is transferred from the surface to the fluid through conduction. On the other hand, the thermal boundary-layer thickness increases, because of the heat transport in the fluid due to enhanced convection process all around the cylinder, which is evident from Figure 1. It is also observed from Figure 3 that the temperature at the surface decreases as κ increases. This is because the

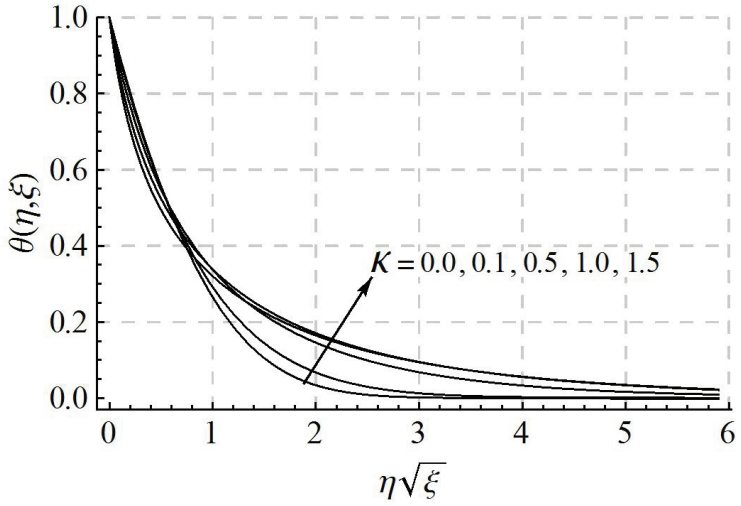

FIG. 2: Effects of the parameter κ on the temperature profile (PST case), when $\mathrm{Pr} = 0.7$, $\xi = 0.3$, and $n = 1.0$ are fixed.

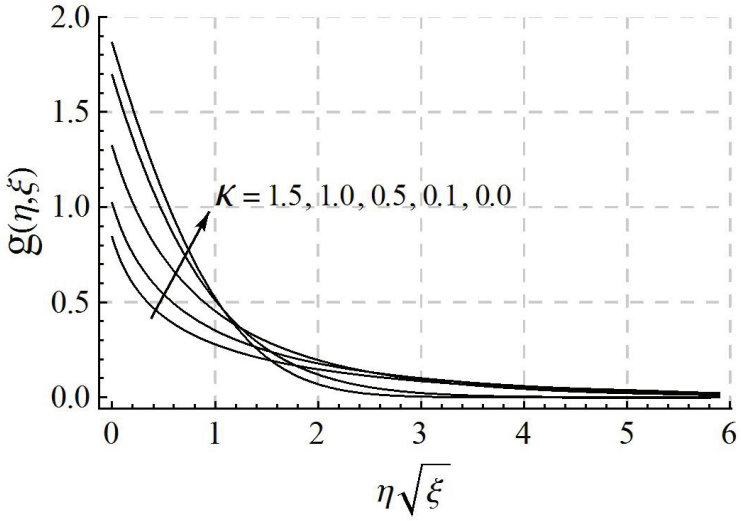

FIG. 3: Effects of the parameter κ on the temperature profile (PHF case), when $\mathrm{Pr} = 0.7$, $\xi = 0.3$, and $n = 1.0$ are fixed.

heat flux is directly proportional to the surface area.

Figure 4 is plotted to examine the consequence of κ and t on the coefficient of skin friction C_f. It is noticed that as time increases the skin friction decreases, which is due to the fact that initially the fluid offers immense resistance to the motion, but as time passes this resistive force reduces and becomes constant as the steady state is achieved. It

is further noticed from Figure 4 that as κ increases the wall skin friction also increases. This is because the velocity gradient at the surface of a cylinder is larger compared to that of a flat plate. The numerical values of the skin friction are illustrated in Table III.

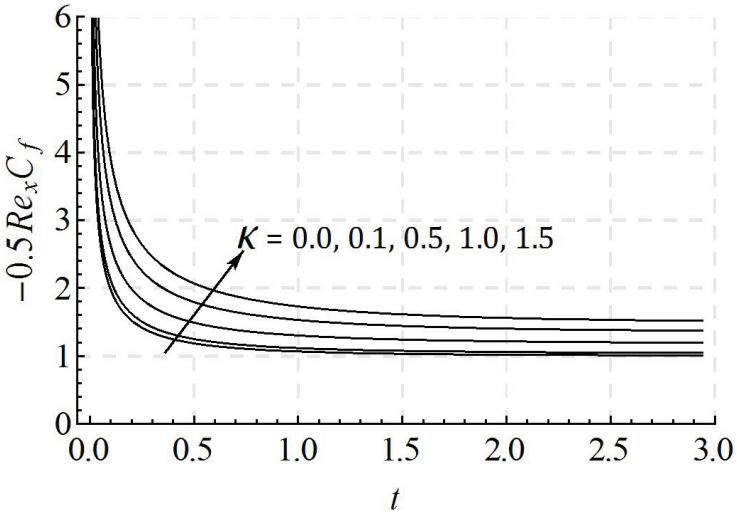

FIG. 4: Effect of the parameter κ on the wall skin friction coefficient.

Figures 5 and 6 demonstrate that an increase in κ raises the Nusselt number, which shows that the convective heat transfer rate due to a slim cylinder is more significant than that of a cylinder with small curvature or a flat plate. The corresponding numerical values of the Nusselt number for various values of Pr, κ, and ξ are shown in Tables IV and V.

The effect of time on the velocity and temperature profiles can be analyzed from Figures 7–9. From Figure 7 it is noticed that initially the boundary-layer region is confined very near to the cylinder surface, but as time passes the flow develops and the boundary-layer thickness increases and reaches to a steady state at $t = 6.0$ (roughly). Figures 8 and 9 demonstrate that for small time the thermal boundary-layer is weak, but with the passage of time heat penetrates into the flow regime, and the thermal boundary-layer thickness increases. In Figure 9, decay in the temperature profile at the wall with the passage of time is due to the decreasing wall heat flux.

To inspect the cooling of the cylinder, the temperature profiles for both the PST and PHF cases are plotted for different values of the Prandtl number in Figures 10 and 11, respectively. From the figures it is observed that as Pr increases the thermal boundary-layer thickness decreases rapidly, and the effects of heat are confined very near to the cylinder surface. It can also be examined from the figures that the fluids with small Pr, such as a metallic fluid (mercury) and gases (helium and air), impede the cooling process as compared to liquid fluids having a large Pr, such as ammonia, Freon, and water. This behavior of the temperature profile shows that the Prandtl number is an important parameter that monitors the cooling process, and the fluids with high Pr, such as oils and lubricants are excellent coolants.

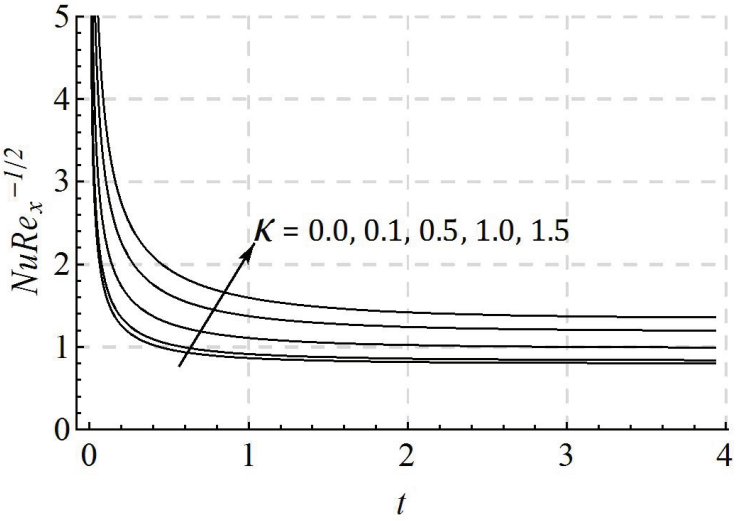

FIG. 5: Effect of the parameter κ on the Nusselt number (PST case), when Pr = 0.7 is fixed.

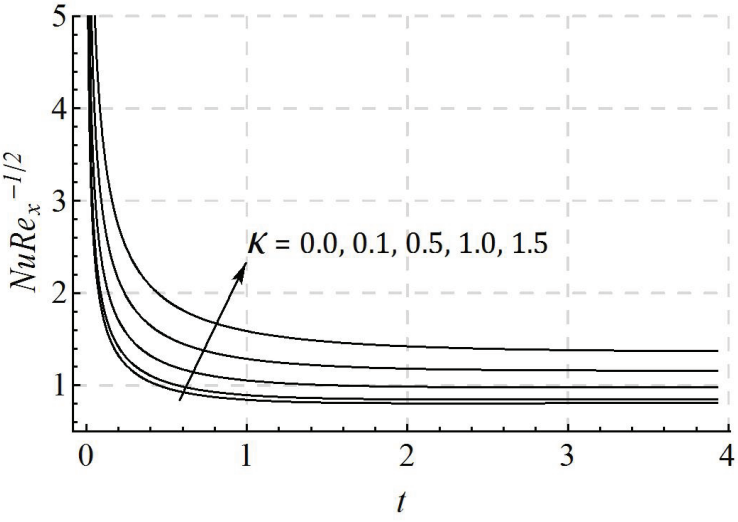

FIG. 6: Effect of the parameter κ on the Nusselt number (PHF case), when Pr = 0.7 is fixed.

Figures 12 and 13 are plotted to show the effect of Pr on the Nusselt number for both types of thermal boundary conditions. It is observed that the Nusselt number increases as Pr increases. This behavior of the Nusselt number shows that convection the fluids with large Pr is more efficient than that of the fluids with small Pr.

Finally, the effects of parameter n on the temperature profiles for both cases (PST and PHF) are illustrated in Figures 14 and 15, respectively. The figures demonstrate that the temperature profile decreases as n increases by leaving no significant consequences on the

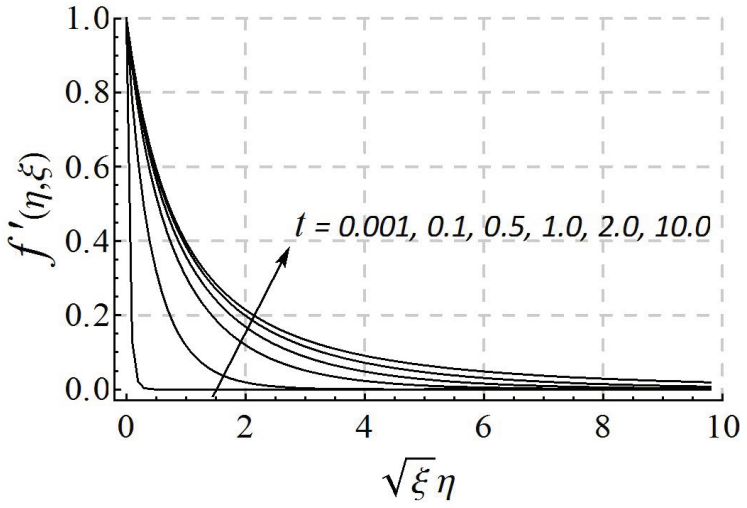

FIG. 7: Effect of dimensionless time t on the velocity profile when $\kappa = 0.5$ is fixed.

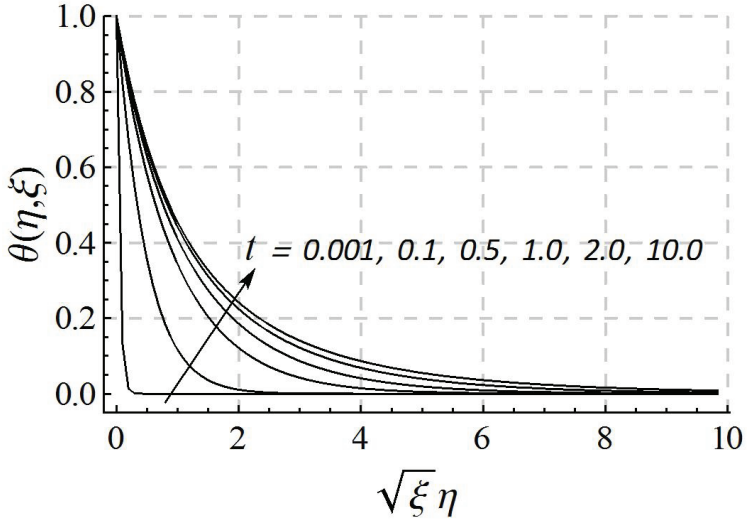

FIG. 8: Effect of dimensionless time t on the temperature profile (PST case) when $\kappa = 0.5$, $n = 1.0$, and $\mathrm{Pr} = 0.7$ are fixed.

thermal boundary-layer thickness. The Nusselt number for different values of the parameter n is depicted in Figures 16 and 17. It is noticed that the Nusselt number increases as the value of n increases.

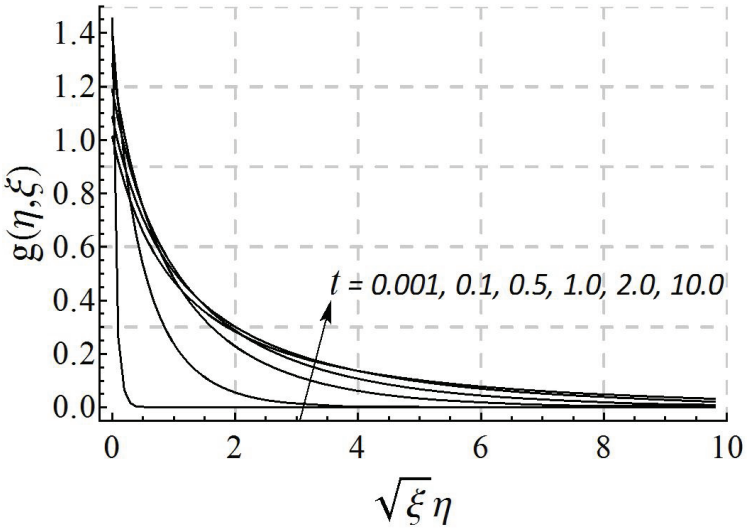

FIG. 9: Effect of dimensionless time t on the temperature profile (PHF case) when $\kappa = 0.5$, $n = 1.0$, and $\mathrm{Pr} = 0.7$ are fixed.

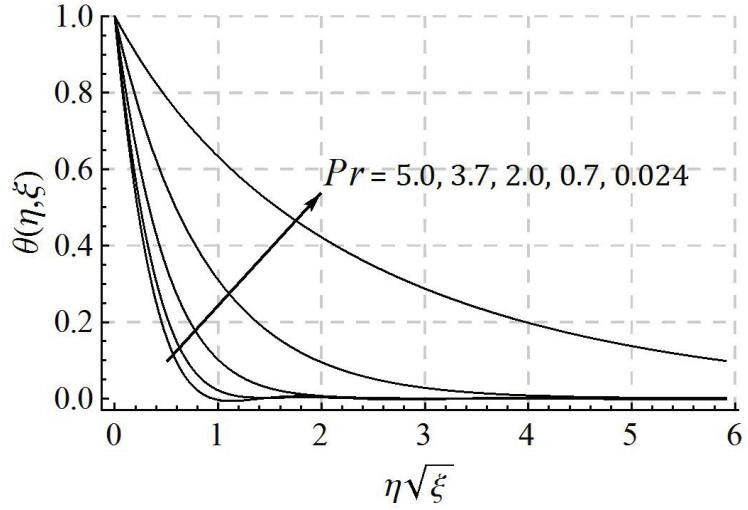

FIG. 10: Effect of Pr on the temperature profile (PST case) when $\kappa = 0.2$, $n = 1.0$, and $\xi = 0.3$ are fixed.

VI. CONCLUDING REMARKS

In this study, the unsteady laminar boundary-layer flow and heat transfer of a viscous fluid over a uniformly stretching cylinder has been investigated. The objectives of this analytic study are to find the best analytic solution for the nonlinear partial differ-

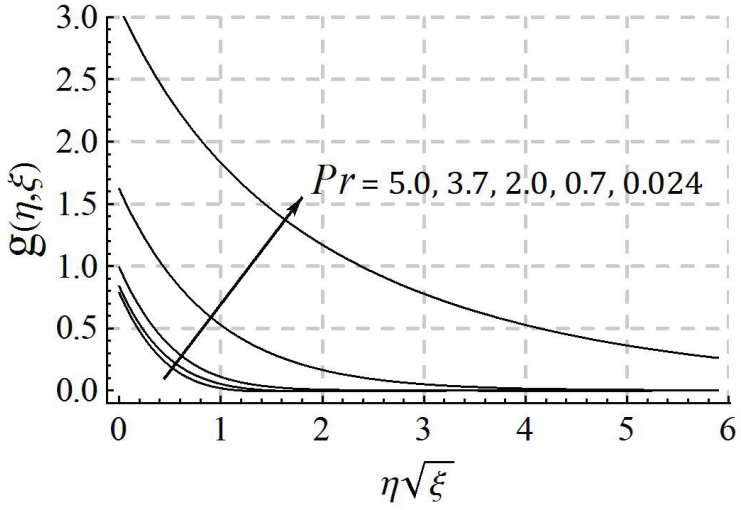

FIG. 11: Effect of Pr on the temperature profile (PHF case) when $\kappa = 0.2$, $n = 1.0$, and $\xi = 0.3$ are fixed.

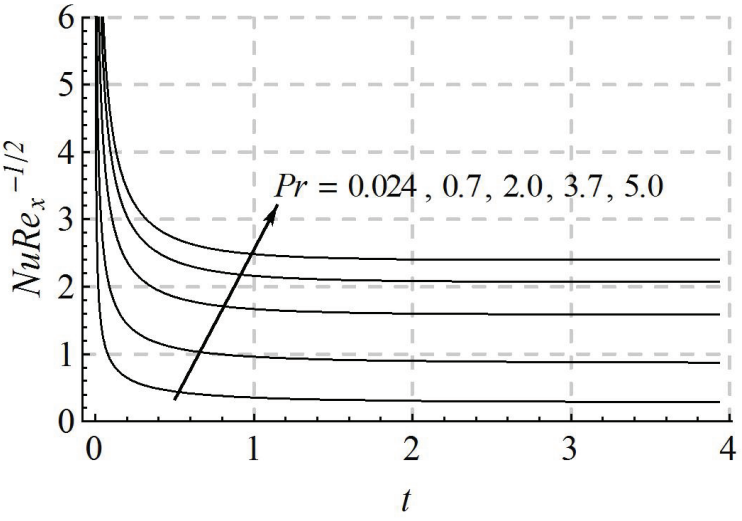

FIG. 12: Effect of Pr on the Nusselt number (PST case), when $\kappa = 0.2$, $\xi = 0.3$, and $n = 1.0$ are fixed.

ential equations, and also to explore the physical aspects of flow and heat transfer with two types of thermal boundary conditions, namely, PST and PHF. We use the homotopy analysis method HAM to find out the analytic solutions of the highly nonlinear partial differential equations, which is valid for all values of time $0 \leq t < \infty$. It is conclude that the boundary-layer thicknesses for both the velocity and temperature fields are strongly

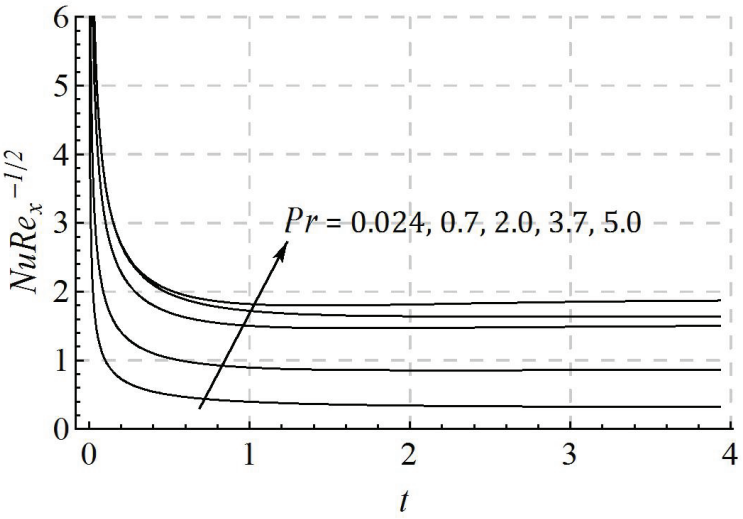

FIG. 13: Effect of Pr on the Nusselt number (PHF case), when $\kappa = 0.2$, $\xi = 0.3$, and $n = 1.0$ are fixed.

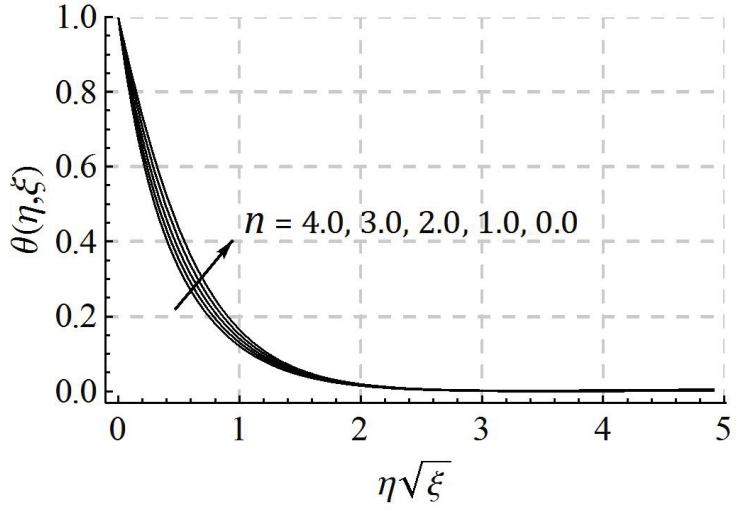

FIG. 14: Effect of parameter n on the temperature profile (PST case) when $\kappa = 0.2$, Pr = 1.5, and $\xi = 0.3$ are fixed.

dependent upon the curvature parameter κ, the Prandtl number Pr, and time. It is observed that the involvement of the curvature parameter in the velocity expression affects the velocity significantly in the whole domain. By increasing the curvature parameter the velocity and the temperature profiles at the cylinder decrease, however, both the boundary-layers increase significantly. Also an increase in curvature parameter causes an increment

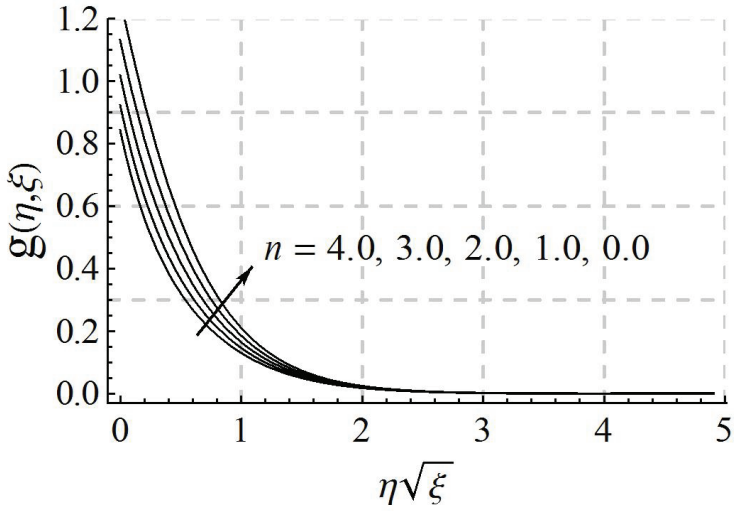

FIG. 15: Effect of parameter n on the temperature profile (PST case) when $\kappa = 0.2$, $\mathrm{Pr} = 1.5$, and $\xi = 0.3$ are fixed.

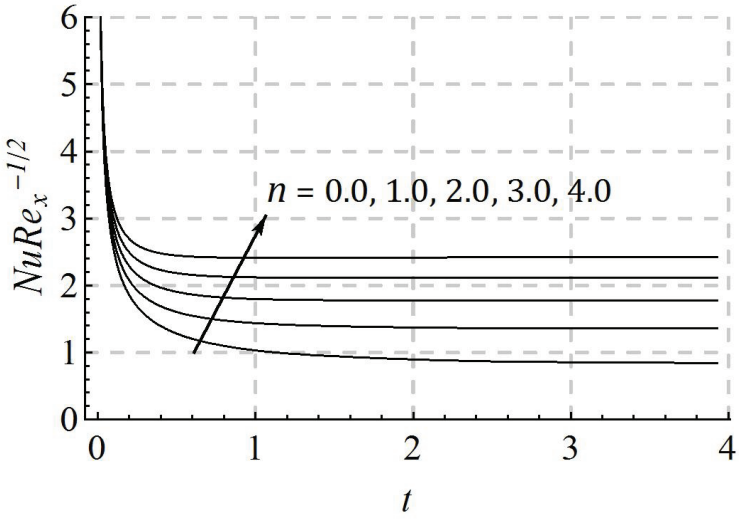

FIG. 16: Effect of parameter n on the Nusselt number (PST case), when $\kappa = 0.2$, $\xi = 0.3$, and $\mathrm{Pr} = 1.5$ are fixed.

in the skin fiction. It is also noticed that the said parameters play an important role in the process of heat exchange. As the curvature parameter κ and the Prandtl number Pr increase, the rate of heat transfer also augments. It can be seen that the heat exchange due to the cylindrical surface is more significant than that of the flat plate. It is also noticed that as time passes the rate of heat transfer diminishes. It is concluded that the fluids with

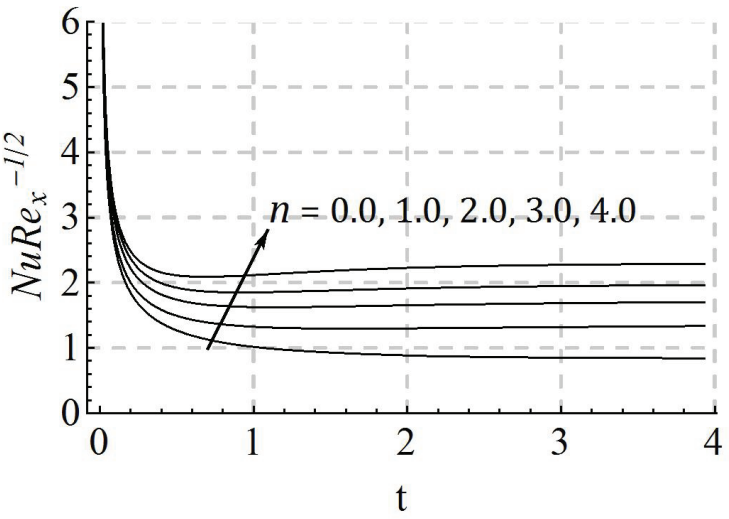

FIG. 17: Effect of parameter n on the Nusselt number (PST case), when $\kappa = 0.2$, $\xi = 0.3$, and $\mathrm{Pr} = 1.5$ are fixed.

large Pr are good coolants, and therefore should be used to enhance the cooling process.

Acknowledgements

The authors are grateful to the anonymous reviewer for his expertise, comments, and suggestions to improve the quality of the manuscript. The authors are also grateful to the Higher Education Commission of Pakistan (HEC) for providing the financial support.

References

[1] E. Pohlhausen, ZAMM **1**, 115 (1921).
[2] B. C. Sakiadis, AIChE J. **7**, 26 (1961).
[3] L. E. Erickson, L. C. Cha, and L. T. Fan, The cooling of a moving continuous flat sheet, (AIChE Chemical Engineering Proc. Symposium, Vol. 62), (8th National Heat Transfer Conference 1965) p.157.
[4] F. K. Tsou, E. M. Sparrow, and R. J. Goldstein, Int. J. Heat Mass Transfer **10**, 219 (1967).
[5] L. J. Crane and Z. Angew, Math. Phys. **21**, 645 (1970).
[6] P. Carragher and L.J. Crane, ZAMM **62**, 564 (1982).
[7] C. Y. Wang, Phys. Fluids, **27**, 1915 (1984).
[8] L. J. Grubka and K. M. Bobba, ASME J. Heat Transfer **107**, 248 (1985).
[9] M. E. Ali, Wärme Stoffäbertrag. **29**, 227 (1994).
[10] E. M. A. Elbashbeshy, J. Phys. D: Appl. Phys. **31**, 1951 (1998).
[11] M. Kumari, H. S. Takhar, and G. Nath, Wärme Stoffübertrag. **25**, 331 (1990).
[12] R. Cortell, Appl. Math. Comp. **184**, 864 (2007).

[13] A. Ali, A. Mehmood, Commun. Nonlinear Sci. Numer. Simulat. **13**, 340 (2008).
[14] C. Y. Wang, Phys. Fluids **31**, 466 (1988).
[15] H. I. Burde, PMM USSR **53**, 271 (1989).
[16] A. Ishak and R. Nazar, Eur. J. Sci. Res. **36**, 22 (2009).
[17] A. Ishak, R. Nazar, and I. Pop, Eng. Con. Manag. **49**, 3265 (2008).
[18] A. Ishak, R. Nazar, and I. Pop, Appl. Math. Mod. **3**, 2059 (2008).
[19] P. D. Weidman and M. E. Ali, Eur. J. Mech. B Fluids **30**, 129 (2011).
[20] C. D. Surma Devi, H. S. Takhar, and G. Nath, Int. J. Heat Mass Transf. **29**, 1996 (1986).
[21] C. Y. Wang, Q. Appl. Math. **48**, 601 (1990).
[22] I. Pop and T. Y. Na, Mech. Res. Comm. **23**, 413 (1996).
[23] H. Xu and S. J. Liao, J. Non-Newtonian Fluid Mech. **129**, 46 (2005).
[24] S. J. Liao, Commun. Nonlinear Sci. Numer. Simulat. **11**, 326 (2006).
[25] A. Mehmood and A. Ali, Proc. I Mech. Eng. Part G: J. Aero. Eng. **221**, 385 (2007):
[26] A. Mehmood, A. Ali, and T. Shah, Commun. Nonlinear Sci. Numer. Simulat. **13**, 902 (2008).
[27] A. Mehmood, A. Ali, H. S. Takhar, and T. Shah, Acta Mech. **199**, 241 (2008).
[28] A. Mehmood, A. Ali, and T. Shah, Can. J. Phys. **86**, 1079 (2008).
[29] A. Ali and A. Mehmood, Commun. Nonlinear Sci. Numer. Simulat. **13**, 340 (2008).
[30] S. Munawar, A. Mehmood, and A. Ali, Int. J. Phys. Sci. **6**, 7709 (2011).
[31] S. Munawar, A. Mehmood, and A. Ali, Int. J. Numer. Meth. Fluids **70**, 671 (2012)
[32] S. J. Liao, *Beyond Perturbation: Introduction to Homotopy Analysis Method* (Chapman & Hall/CRC Press, London/Boca Raton, 2003).
[33] S. J. Liao, The proposed homotopy analysis technique for the solution of nonlinear problems, (PhD thesis, Shanghai Jiao Tong University; 1994).
[34] S. J. Liao, Int. J. Nonlinear Mech. **32**, 815 (1997).
[35] H. Xu and S. J. Liao, J. Non-Newtonian Fluid Mech. **129**, 46 (2005).
[36] S. J. Liao, Commun. Nonlinear Sci. Numer. Simulat. **11**, 326 (2006).
[37] M. Khan, S. Munawar, and S. Abbasbandy, Int. J. Heat Mass Transf. **53**, 1290 (2010).
[38] A. Mehmood, S. Munawar, and A. Ali, Commun. Nonlinear Sci. Numer. Simulat. **15**, 4233 (2010).
[39] S. Abbasbandy, Int. Commun. Heat Mass Transf. **34**, 380 (2007).
[40] S. J. Liao, Int. J. Non-Linear Mech. **34**, 759 (1999).
[41] S. J. Liao, Commun. Nonlinear Sci. Numer. Simulat. **15**, 2003 (2010).
[42] J. C. William and T. H. Rhyne, SIAM J. Appl. Math. **38**, 215 (1980).